J. Fluid Mech. (1970), *vol.* 40, *part* 4, *pp.* 685–704
Printed in Great Britain

Low Reynolds number shear flow past a rotating circular cylinder. Part 1. Momentum transfer

By C. R. ROBERTSON† AND A. ACRIVOS
Department of Chemical Engineering, Stanford University

(Received 16 June 1969)

The two-dimensional flow of an incompressible viscous fluid past a circular cylinder, symmetrically placed in a uniform shear field, is considered both theoretically and experimentally for small values of the shear Reynolds number. A series of angular rotational speeds is covered, each giving rise to a fundamentally different flow pattern. It is shown first that the Stokes solution to this problem is not entirely consistent everywhere with the linear shear boundary condition which presumably exists far from the body. Using the method of inner and outer expansions, this solution is then improved by properly taking into account the first-order effects of the inertia terms, but, surprisingly, the streamline structure in the outer region is still found to depart from that of the uniform shear sufficiently far away from the object.

In spite of the somewhat bizarre nature of the theoretical solution far from the cylinder, experimental studies clearly show, however, that it accurately represents the actual flow within the inner region over a wide range of cylinder rotation rates.

1. Introduction

Numerous investigations have appeared in the literature dealing with the motion of small objects suspended in a moving fluid, a subject of central importance to the field of particle dynamics. And yet, the large majority of these studies have been restricted to cases in which the particles, although in principle free to rotate and translate, were assumed to remain stationary relative to a suitably chosen co-ordinate system, the result being that many of the important phenomena arising as a consequence of particle rotation have remained largely unexplored. In fact, the effects of particle rotation appear to have been considered only rather recently, for example by Bretherton (1962), Saffman (1965), Cox, Zia & Mason (1968) and, for the case of heat transfer, by Frankel & Acrivos (1968).

The present study considers in some detail a central problem in this general category, that of the steady, two-dimensional, low Reynolds number motion of an incompressible viscous fluid past a circular cylinder when the velocity at large distances is described by a uniform simple shear, and, in particular, the case in which the cylinder is placed symmetrically in the shear field so that the

† Present address: Marathon Oil Company, Littleton, Colorado.

lift and drag are identically zero. This problem was also treated theoretically by Bretherton (1962), who dealt primarily with the case in which the cylinder is assumed to translate relative to the centre of the shear field thereby experiencing both drag and lift. Thus, although the theoretical part of the present work will be seen to parallel in some respects that of Bretherton's, the respective solutions will be quite distinct unless the Reynolds number is identically zero. In fact, as was already remarked by Bretherton, his analysis for finite Reynolds numbers ceases to apply when the slip velocity is made to vanish. Although, admittedly, the present case might seem rather specialized, it is of considerable interest in its own right in that it refers to the motion of a suspended neutrally buoyant particle which, at steady state, cannot of course support a net force by the surrounding fluid.

As was pointed out by Bretherton (1962), the present problem admits a Stokes solution, satisfying all the boundary conditions, for arbitrary rotational speeds of the cylinder. At first glance, this Stokes solution appears to be everywhere well behaved. However, upon closer examination, it will be shown to predict a flow pattern far from the cylinder which differs, in some important respects, from that of the imposed constant shear, thus creating some doubt as to whether the Stokes solution truly represents the flow field for vanishingly small Reynolds numbers. It was felt desirable, therefore, to investigate this problem somewhat further and in more detail for the purpose of developing a proper low-Reynolds-number asymptotic solution which would apply everywhere in the flow domain.

As will be seen below, this was accomplished using the method of inner and outer expansions, according to which the flow field is thought of as consisting of two distinct but overlapping domains: an 'inner' region, within which the inertia forces are small in comparison with the viscous terms, and an 'outer' region in which both inertia and viscous forces are of comparable magnitude. Separate solutions are then obtained for the two domains which are matched in the region of overlap.

Following this procedure, appropriate inner and outer solutions were constructed which will be shown to satisfy all the imposed boundary conditions and matching requirements. In addition, the Stokes solution in the inner region was extended to include the first-order correction terms arising from the presence of inertia. Nevertheless, it will be shown that the flow pattern at large distances from the cylinder still retains some of the peculiar features of the Stokes solution in that it includes a secondary motion which, although weak, is of sufficient magnitude to overshadow the uniform simple shear in certain regions of the far outer field.

To test the theoretical predictions, an experimental programme was undertaken in which the flow past a circular cylinder symmetrically placed in a linear shear field was examined in considerable detail for small values of the Reynolds number. A series of cylinder rotational speeds were considered each giving rise to a fundamentally different streamline pattern. Although, owing to equipment limitations, attention had to be restricted to the inner region, it will be seen that, in every case studied, the experimental results were found to be in excellent agreement with the theoretical analysis based on the Stokes solution.

2. The Stokes solution

In the absence of inertia terms, the Navier–Stokes equation in terms of the stream function ψ reduces to

$$\nabla^4\psi = 0, \quad r > 1. \tag{1}$$

As shown by Bretherton (1962), the appropriate solution satisfying the boundary conditions

$$\psi = 0, \quad u_\theta \equiv -\partial\psi/\partial r = -\Omega \quad \text{at} \quad r = 1, \tag{2}$$

$$\psi \to \tfrac{1}{2}r^2\sin^2\theta \equiv \tfrac{1}{2}y^2 \quad \text{as} \quad r \to \infty, \tag{3}$$

is

$$\psi(r,\theta) = \tfrac{1}{2}y^2 - \tfrac{1}{4}\{2(1-2\Omega)\ln r + 1 + ([1/r^2]-2)\cos 2\theta\}, \tag{4}$$

where r and θ are the usual cylindrical polar co-ordinates with the origin placed along $y = 0$, the line of symmetry of the undisturbed shear field. In these and all subsequent expressions, the variables have been rendered dimensionless using a, the radius of the cylinder, as the characteristic length, and Sa as the characteristic velocity, with S being the value of the *dimensional* shear rate which applies far from the cylinder. As mentioned above, the present analysis will be restricted to the case in which the cylinder is placed symmetrically in the shear field so that both lift and drag are identically zero. Also, as can be verified by direct substitution, the speed of rotation Ω is related to $\mathbf{t}$, the dimensionless torque per unit length exerted by the fluid on the cylinder, by means of

$$\mathbf{t} = -(2\pi\mathbf{k}/R)(1-2\Omega), \tag{5}$$

where

$$R \equiv Sa^2/\nu \tag{6}$$

is the Reynolds number of the motion, with ν being the kinematic viscosity of the fluid. Clearly, in view of (5), the dimensionless angular speed of a freely rotating cylinder is $\Omega = \frac{1}{2}$.

Up to now, it would seem that the general solution, as given by (4) for arbitrary rotational speeds Ω, has been accepted as a bona fide Stokes solution, falling into the same category as the familiar solutions for uniform creeping flow past a sphere or any other finite body, in the sense that all the imposed boundary conditions appear to have been satisfied exactly. Nevertheless, the behaviour of (4) for large values of r is sufficiently bizarre to warrant further attention. Thus, for $r \gg 1$ and $\Omega \neq \frac{1}{2}$, the creeping-flow solution reduces to

$$\psi \to \tfrac{1}{2}y^2 - \tfrac{1}{2}(1-2\Omega)\ln r, \tag{7}$$

which is seen to consist of two terms: the impressed uniform shear, and a 'point-vortex' flow which, although vanishingly small as $r \to \infty$, clearly dominates for small enough values of y. The consequences resulting from the presence of the logarithmic term in (7) are as follows: for $0 \leqslant \Omega < \frac{1}{2}$, (7) predicts the existence of two wakes, i.e. regions of negative ψ, on either side of the cylinder, each having a width which increases with r as

$$2((1-2\Omega)\ln r)^{\frac{1}{2}}.$$

In contrast, for $\Omega > \frac{1}{2}$, all the streamlines given by (7) are easily shown to cross the x-axis, thereby suggesting that all the streamlines must close.

To be sure, the rather unexpected streamline pattern that arises, according to (7), for sufficiently large r and $\Omega \neq \frac{1}{2}$ may not appear, at first glance, to be of any great significance since the velocities associated with the secondary motion are seen to decay as r^{-1}. Yet, the creeping flow solution would imply, for example, that, in the presence of a stationary cylinder, a fluid particle originally released anywhere within the wake $x < 0$, $0 < y < (\ln r)^{\frac{1}{2}}$, $r \gg 1$, would remain within the half-plane $x < 0$, and would eventually end up inside the quadrant $x < 0$, $-(\ln r)^{\frac{1}{2}} < y < 0$. On the other hand, for $\Omega > \frac{1}{2}$, any fluid particle within the whole flow domain would, according to (4), circumvent the cylinder and return ultimately to its original position owing to the fact that all the streamlines are closed. Clearly, these particle paths, besides being in sharp contrast to those in a uniform simple shear, appear to be highly paradoxical, since they indicate that the presence of a small cylinder will exert a very real influence on the flow structure throughout large regions of the domain, even those extending to infinity. Thus, it would seem that, for $\Omega \neq \frac{1}{2}$, the behaviour of the creeping flow solution at large distances from the cylinder is incompatible with that of a real fluid system.

The case $\Omega = \frac{1}{2}$, corresponding to a freely rotating cylinder, merits special attention. Here, the appropriate limit of (4) for large r and $\theta \to 0$ (y fixed) is

$$\psi \to \tfrac{1}{2}y^2 + \tfrac{1}{4}(1 - [1/r^2]), \tag{8}$$

implying that r is finite, at $y = 0$, for $0 \leqslant \psi < \frac{1}{4}$; consequently, all the streamlines within this range of ψ must eventually close. However, since the width of this region of closed streamlines vanishes with increasing r as $\sqrt{(2)}/r$, whereas, from (8), $\psi \to \frac{1}{2}y^2 + \frac{1}{4}$ for $\psi \geqslant \frac{1}{4}$, it would appear that, for the special case $\Omega = \frac{1}{2}$, the condition of uniform shear at infinity is satisfied everywhere by the Stokes solution.

At any rate, for $\Omega \neq \frac{1}{2}$, some fundamental questions remain regarding the validity of the Stokes solution far from the object. Admittedly, the seemingly paradoxical behaviour described earlier is rather mild when compared with some of the classical examples that have been treated in the literature, such as the well-known Stokes paradox for an infinite stationary cylinder in a uniform flow at vanishingly small Reynolds numbers. Nevertheless, it was felt desirable to try and resolve this matter.

By analogy with most low Reynolds number problems of a similar type, it seemed logical to suppose at the outset that the apparent inconsistency at infinity could be removed if the inertia terms were taken into account, since inertial and viscous forces are of comparable magnitude at large distances from the object. Hence, the creeping flow analysis was extended to include the first-order contribution of these inertial effects. This was accomplished in a systematic way using the technique of inner and outer expansions as presented, for example, by Proudman & Pearson (1957) and by Bretherton (1962).

3. The solution for non-zero Reynolds numbers

Following the well-established procedure of inner and outer expansions, we assume that as $R \to 0$ the flow domain around the cylinder divides into two separate but overlapping regimes. In the first, the so-called Stokes region, the stream function ψ satisfies

$$\nabla^4\psi = \frac{R}{r}\left\{\frac{\partial\psi}{\partial\theta}\frac{\partial\nabla^2\psi}{\partial r} - \frac{\partial\psi}{\partial r}\frac{\partial\nabla^2\psi}{\partial\theta}\right\}, \tag{9}$$

with boundary conditions

$$\psi = 0, \quad \partial\psi/\partial r = \Omega \quad \text{at} \quad r = 1.$$

In the outer, or so-called Oseen, region the basic equation becomes

$$\nabla^4\Psi = \frac{\partial\Psi}{\partial\eta}\frac{\partial\nabla^2\Psi}{\partial\xi} - \frac{\partial\Psi}{\partial\xi}\frac{\partial\nabla^2\Psi}{\partial\eta}, \tag{10}$$

with $\partial\Psi/\partial\eta \to \eta$ as $\rho \to \infty$, where, following Bretherton (1962), the strained co-ordinates

$$(\rho, \theta) = (R^{\frac{1}{2}}r, \theta), \quad \xi = R^{\frac{1}{2}}x, \quad \eta = R^{\frac{1}{2}}y, \quad \Psi(\xi, \eta) = \Psi(\rho, \theta) = R\psi(r, \theta)$$

have been introduced. Clearly, (10) reflects the proper balance between the inertial and viscous forces which is presumed to exist at large distances from the cylinder, i.e. for $r > O(R^{-\frac{1}{2}})$.

Next we seek a solution of the form

$$\psi(R, r, \theta) = \sum_{n=0}^{\infty} f_n(R)\,\psi_n(r, \theta), \quad \Psi(R, \rho, \theta) = \sum_{n=0}^{\infty} F_n(R)\,\Psi_n(\rho, \theta),$$

where

$$\frac{f_{n+1}(R)}{f_n(R)}, \quad \frac{F_{n+1}(R)}{F_n(R)} \to 0 \quad \text{as} \quad R \to 0,$$

and require that the two expressions for ψ satisfying, respectively, (9) and (10) should match within the intermediate region $r \to \infty$, $\rho \to 0$. By inspection, the, first term of the outer solution is

$$\Psi_0(\rho, \theta) = \tfrac{1}{2}\eta^2 = \tfrac{1}{2}\rho^2\sin^2\theta, \quad F_0(R) = 1,$$

whereas that for the inner expansion is the Stokes solution, (4), which, with $f_0(R) = 1$, is seen to fulfil the matching requirement for sufficient small R.

The next two terms of the outer solution are now determined by the form of $\psi_0(r, \theta)$ which, within the overlap region, becomes

$$R\psi_0(r, \theta) \underset{r\to\infty}{\to} \tfrac{1}{2}\rho^2\sin^2\theta + \tfrac{1}{4}R\ln R(1-2\Omega) - \tfrac{1}{4}R\{2(1-2\Omega)\ln\rho + 1 - 2\cos 2\theta\} + \ldots. \tag{11}$$

Therefore,

$$\Psi(R, \rho, \theta) = \tfrac{1}{2}\rho^2\sin^2\theta + \tfrac{1}{4}R\ln R(1-2\Omega) + R\Psi_2(\rho, \theta) + \ldots,$$

where Ψ_2 can easily be seen to satisfy

$$\eta\frac{\partial}{\partial\xi}(\nabla^2\Psi_2) = \nabla^4\Psi_2, \quad \nabla^2\Psi_2 \to 0 \quad \text{as} \quad \rho \to \infty. \tag{12}$$

This will be recognized as an Oseen-type equation in which the equations of motion have been linearized about the uniform simple shear.

As shown by Bretherton (1962), the fundamental solution ω of $\eta(\partial\omega/\partial\xi) = \nabla^2\omega$, having the required logarithmic singularity at the origin, is

$$\omega = \int_0^\infty \frac{dt}{2t(1+t^2/12)^{\frac{1}{2}}} \exp - \left\{\frac{\xi^2 - \xi\eta t + \eta^2(1+t^2/3)}{4t(1+t^2/12)}\right\}, \tag{13}$$

with $\omega \to -\ln\rho + 1{\cdot}372$ as $\rho \to 0$.

This of course is not quite the desired solution to the present problem, since, owing to the fact that

$$\nabla^2\Psi_0' = 1 - \frac{2\cos 2\theta}{r^2},$$

a solution to (12) is being sought which, as $\rho \to 0$, becomes

$$\nabla^2\Psi_2' \to -\frac{2\cos 2\theta}{\rho^2}.$$

However, noting that $\partial^2\omega/\partial\xi^2$ is also a solution to (12) and that

$$-\frac{\partial^2}{\partial\xi^2}\ln\rho = \frac{\cos 2\theta}{\rho^2},$$

it can be seen immediately that

$$\nabla^2\Psi_2' = -2\frac{\partial^2\omega}{\partial\xi^2}, \tag{14}$$

a particular solution to which, Ψ_2^p, is (Bretherton 1962; Morse & Feshbach 1953)

$$\Psi_2^p = -\frac{1}{\pi}\int_0^\infty \int_0^{2\pi} \ln|\boldsymbol{\rho} - \boldsymbol{\rho}_0| \frac{\partial^2\omega}{\partial\xi_0^2}\rho_0\, d\rho_0\, d\theta_0. \tag{15}$$

Although the integral appearing in (15) cannot be evaluated analytically, it is possible to obtain asymptotic expressions for Ψ_2^p, for small and for large values of ρ, which, as will become apparent shortly, lead to a rather complete description of the flow field far from the cylinder as well as to an improved solution in the Stokes region. The detailed and rather involved mathematical manipulations leading to these asymptotic expressions have been given by Robertson (1969) and are available from the authors on request, so that only the results will be presented below.

4. The Stokes region

It can be shown, Robertson (1969), that the asymptotic form of Ψ_2^p, as given by (15), becomes, for small values of ρ,

$$\Psi_2^p = \tfrac{1}{2}\cos 2\theta - 0{\cdot}9101 + \tfrac{1}{8}\rho^2\ln\rho\sin 2\theta - \rho^2\{0{\cdot}07216 - 0{\cdot}08275\sin 2\theta + 0{\cdot}08297\cos 2\theta - \tfrac{1}{96}\sin 4\theta\} + O(\rho^4\ln\rho). \tag{16}$$

To this must be added the homogeneous solution of (14)

$$\Psi_2^h = -\tfrac{1}{2}(1-2\Omega)\ln\rho + 0{\cdot}6601$$

in order that the outer solution match with ψ_0 as given by (11). Therefore, the first three terms of the outer solution become

$$\Psi = \tfrac{1}{2}\rho^2 \sin^2\theta + \tfrac{1}{4}R\ln R(1-2\Omega) + R\{-\tfrac{1}{2}(1-2\Omega)\ln\rho + 0{\cdot}6601 + \Psi_2^p\} + o(R). \quad (17)$$

Returning now to the inner region, we see that, owing to the presence of the $\rho^2\ln\rho$ term in (16), the Stokes expansion must assume the form

$$\psi = \psi_0 + R\ln R\psi_1 + R\psi_2 + o(R), \quad (18)$$

which, when substituted into (9), results in

$$\nabla^4\psi_1 = 0,$$

and

$$\nabla^4\psi_2 = \frac{1}{r}\left\{\frac{\partial\psi_0}{\partial\theta}\frac{\partial\nabla^2\psi_0}{\partial r} - \frac{\partial\psi_0}{\partial r}\frac{\partial\nabla^2\psi_0}{\partial\theta}\right\} = 2\left\{\left(\frac{1-2\Omega}{r^4} - \frac{1}{r^2}\right)\sin 2\theta + \left(\frac{1}{r^2} - \frac{1}{r^4}\right)\sin 4\theta\right\},$$

with boundary conditions $\psi_{1,2} = 0$, $\partial\psi_{1,2}/\partial r = 0$ at $r = 1$. In addition, because of (16), the matching requirement yields the condition that

$$\psi_1 \to \tfrac{1}{16}r^2\sin 2\theta \quad \text{as} \quad r\to\infty,$$

and

$$\psi_2 \to r^2\{\tfrac{1}{8}\ln r\sin 2\theta - 0{\cdot}07216 + 0{\cdot}08275\sin 2\theta - 0{\cdot}08297\cos 2\theta + (\sin 4\theta)/96\} \quad \text{as} \quad r\to\infty.$$

The appropriate solutions are (Robertson 1969)

$$\psi_1 = \tfrac{1}{16}(r^2 - 2 + [1/r^2])\sin 2\theta \quad (19)$$

and

$$\psi_2 = -0{\cdot}07216(r^2 - 2\ln r - 1) + \left(r^2 - 2 + \frac{1}{r^2}\right)(0{\cdot}08275\sin 2\theta - 0{\cdot}08297\cos 2\theta) + \left(r^2 - 1 - \frac{1}{r^2} + \frac{1}{r^4}\right)\frac{\sin 4\theta}{96} + (r^2 + 1 - 2\Omega)\frac{\ln r\sin 2\theta}{8} - \frac{1-\Omega}{8}\left(1 - \frac{1}{r^2}\right)\sin 2\theta. \quad (20)$$

Therefore, the inner solution up to but not including terms $O(R^2\ln R)$ is (18), with ψ_0, ψ_1 and ψ_2 given, respectively, by (4), (19) and (20).

A bulk property of particular interest here is $\mathbf{t}$, the dimensionless torque per unit length acting on the cylinder. This is given by

$$\mathbf{t} = -\int_S \mathbf{n}.(\mathsf{T} - \mathbf{uu}) \wedge \mathbf{r}\,ds, \quad (21)$$

where T is the dimensionless stress tensor, S any contour enclosing the cylinder and $\mathbf{n}$ the unit outer normal on the line element ds. Applying (21) on the surface of the cylinder, $r = 1$, and expressing T and $\mathbf{u}$ in terms of the stream function results in

$$\mathbf{t} = \frac{2\pi\mathbf{k}}{R}\left\{\Omega - \frac{1}{2\pi}\int_0^{2\pi}\left(\frac{\partial^2\psi}{\partial r^2}\right)_{r=1} d\theta\right\},$$

which, on account of (18), (4), (19) and (20), reduces to

$$\mathbf{t} = -\frac{2\pi\mathbf{k}}{R}(1 - 2\Omega - 0{\cdot}2886R + O(R^2\ln R)).$$

Therefore, the dimensionless angular speed Ω for a freely rotating cylinder becomes

$$\Omega = \tfrac{1}{2}[1 - 0{\cdot}2886R + O(R^2 \ln R)], \quad \text{for} \quad \mathbf{t} = 0.$$

Clearly, these last two expressions indicate that the inclusion of inertia effects in the analysis leads to a lower torque and a lower rotational speed of the cylinder, relative to those obtained on the basis of the creeping flow solution alone.

In closing, it should be noted that (17) and (18), the two solutions obtained here for, respectively, the outer and inner regions, differ in a fundamental way from those developed by Bretherton (1962), which, owing to the presence of a finite cylinder velocity, were determined only to order $R^{\frac{1}{2}} \ln R^{\frac{1}{2}}$.

5. The Oseen region

The successful matching between the first three terms of the inner solution and (17) gives rise to some confidence that the technique used to linearize the equations of motion in the outer region about the uniform simple shear solution is a valid one for small enough Reynolds numbers. Hence, it should be possible to obtain the structure of the far field by examining the asymptotic expansion of (17) as $\rho \to \infty$. As shown by Robertson (1969), this takes the form

$$\Psi = \tfrac{1}{2}\rho^2 \sin^2\theta + \tfrac{1}{4}R \ln R(1-2\Omega) + R\left\{-\tfrac{1}{2}(1-2\Omega)\ln\rho + 0{\cdot}6601 - \ln\rho - \frac{0{\cdot}9511}{\rho^{\frac{4}{3}}} + \frac{1{\cdot}5218\cos 2\theta}{\rho^{\frac{4}{3}}} - \frac{2\sin 2\theta}{\rho^2} + O(\rho^{-\frac{8}{3}})\right\} + O(R^2 \ln R). \tag{22}$$

Off hand, it would appear that the above expression might be incompatible with the requirement that angular momentum be conserved, since, if $\mathbf{t}$ is evaluated according to (21) by choosing for a contour a large circle of radius $\rho \gg 1$, the presence of the second logarithmic term in (22) will lead to an additional viscous contribution to the torque which is absent if (21) is computed on the surface of the cylinder using (4). Nevertheless, when the inertial part of (21) is taken into account, the interaction between the term in (22) involving $\sin 2\theta$ with the uniform shear leads to the only non-zero inertial contribution to $\mathbf{t}$ which exactly cancels the extra viscous term described above. Hence, (5) is recovered so that, in this respect at any rate, (22) is a consistent result.

What is very surprising about (22), however, is that at large ρ

$$\Psi \underset{\rho\to\infty}{\to} \tfrac{1}{2}\eta^2 - \tfrac{1}{2}R(3-2\Omega)\ln\rho + \tfrac{1}{4}R\ln R(1-2\Omega) + 0{\cdot}6601R, \tag{23}$$

which is seen to be effectively identical with the large r expansion of the inner solution, equation (7), except for a difference in the coefficient of the logarithmic term. Thus, it is evident that all the peculiar features of the Stokes solution at large r, which were discussed in some detail in § 2, are still retained in the far outer field even when inertial effects are taken into account. In fact, when $0 \leqslant \Omega < \frac{3}{2}$, the streamline pattern for $\rho \gg 1$ is qualitatively similar to that in the Stokes region for $0 \leqslant \Omega < \frac{1}{2}$ and $r \gg 1$; likewise, for $\Omega = \frac{3}{2}$ and $\Omega > \frac{3}{2}$, the streamlines in the outer flow have the same characteristic features as those in the inner

region when $\Omega = \frac{1}{2}$ and $\Omega > \frac{1}{2}$, respectively. As before, these three angular speed ranges correspond to different signs in the coefficient of the logarithmic term; however, owing to the presence of the additional logarithmic term in (22), the angular speed required to completely eliminate the two wakes from the Oseen region is now $\Omega = \frac{3}{2}$, rather than $\Omega = \frac{1}{2}$ as was the case earlier with the Stokes solution. This indicates, for example, that, when $\Omega = \frac{1}{2}$, the wakes will have been swept out from the inner into the outer region where they will still persist until Ω is increased to $\frac{3}{2}$, at which point the wakes will disappear altogether.

It would appear, therefore, that, in the case of a truly two-dimensional flow past an infinite circular cylinder, one should not require the streamline structure at infinity to conform everywhere to that of a uniform simple shear, except when $\Omega = \frac{3}{2}$. However, since the magnitude of the secondary motion becomes extremely small as $\rho \to \infty$, the condition of constant vorticity at infinity will still apply.

6. Experiments

On the basis of past experience with other creeping flow phenomena, one would expect the Stokes solution to provide a very accurate representation of the actual flow pattern near the body for small, but non-zero Reynolds numbers. In fact, Cox, Zia & Mason (1968) have recently shown that, in the case of a freely rotating cylinder ($\Omega = \frac{1}{2}$), the three streamlines $\psi = 0{\cdot}16$, $1{\cdot}67$ and $0{\cdot}25$, the latter corresponding to the boundary of the closed streamline region, are given accurately in the neighbourhood of the cylinder ($1 \leqslant r < 2$) by the appropriate creeping flow solution, (4). However, in view of some of the rather bizarre features of the theoretical solution described in earlier parts of this paper, it seemed desirable to experimentally investigate such flows in more detail, and, in particular, over a more extended region surrounding the cylinder and for a much wider range of rotational speeds Ω than had been attempted hitherto.

Following is a description of the apparatus, the experimental techniques and the results.

The shear flow apparatus

One of the earliest accounts of the design and construction of an instrument solely for the purpose of generating a shear flow is due to Taylor (1923, 1934). Generally speaking, such a shear field may be achieved by means of a 'parallel band' apparatus, a 'four-roller' set-up, or a cylindrical Couette device. The latter has been used extensively in recent years by Mason (1951) to study a wide variety of problems involving particle motions in sheared suspensions (e.g. Darabaner, Raasch & Mason 1967). Also, Giesekus (1962) has investigated in a 'four-roller apparatus' the deformation of small particles bound together with flexible rods. Other applications, however, have been better served by the 'parallel band' set-up, as is evidenced by the work of Robertson (1959), Reichardt (1959), Deardorff (1963), and Kohlman & Mollo-Christensen (1965).

After taking into consideration the advantages and disadvantages of the several types of shear flow generators, it was decided that the 'parallel band'-type arrangement would be most compatible with the goals of the present research

programme. This led to the construction of the shear-flow apparatus shown in figure 1, which represents a larger and more flexible version of a similar device built by Kohlman (1963).

The 'band' assembly consists of timing belts and timing pulleys, built on a tooth grip principle, in which the molded teeth of the oil-resistant rubber belt are designed to make positive engagement with the mating axial grooves on the pulleys. One primary advantage of using timing belt devices is their positive

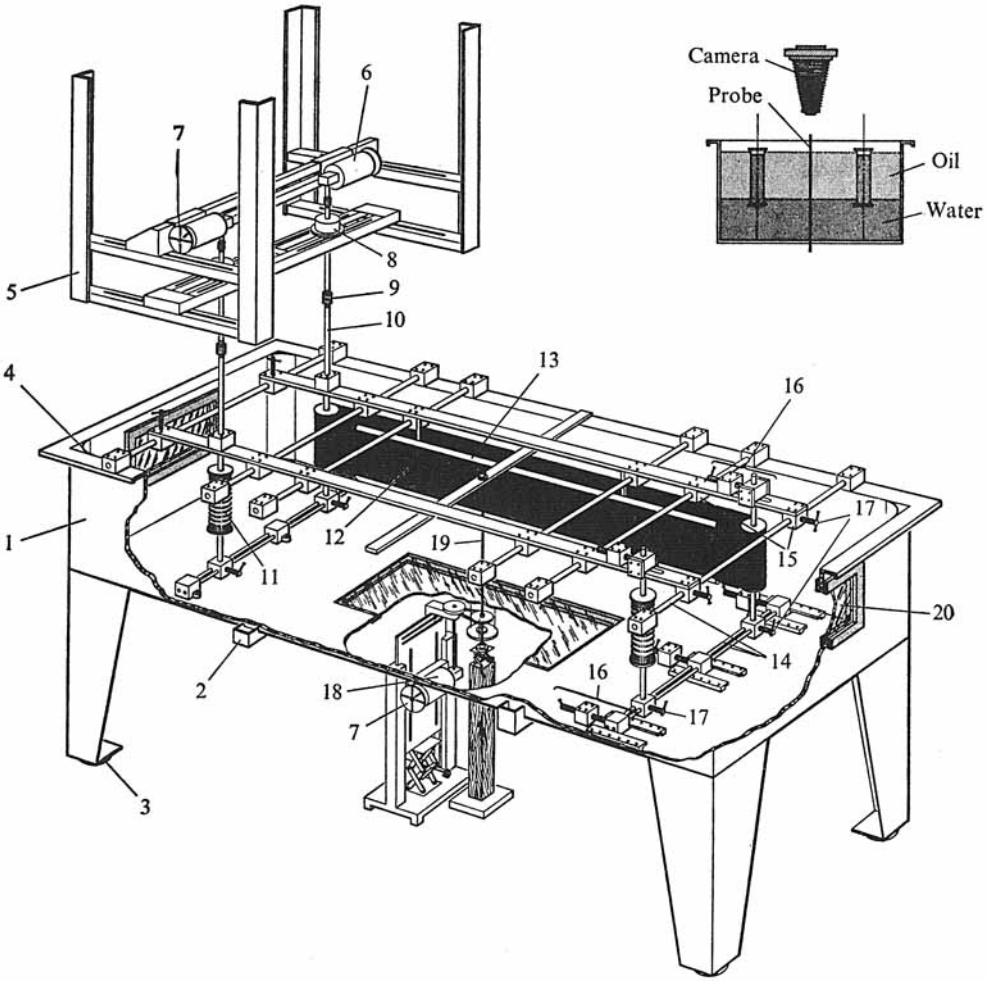

FIGURE 1. Experimental shear-flow apparatus. (1) Shear-flow tank. 10 ft. long, 2 ft. high, 3·5 ft. wide; legs, 37·5 in. high; end windows, 14 in. high, 20 in. wide (viewing area); bottom window, 18 in. wide, 40 in. long (viewing area); material $\frac{3}{16}$ in. steel; exterior and interior coated with coal tar epoxy. (2) Channel supports, steel. (3) Shock absorber, leveller. (4) Contour adjustors: arc segments from a 6 in. radius circular cylinder. (5) Gearmotor and gear reducer support. (6) $\frac{1}{2}$ HP gearmotor. (7) Grooved aluminum disk (lacquered). (8) Helical gear speed reducer. (9) Flexible shaft couplings. (10) 1·5 in. diameter stainless steel pulley shafts. (11) Timing belt pulley. (12) Timing belt (12 in. high). (13) Stainless steel belt support. (14) Stainless steel shafts. (15) Anodized aluminium bearing blocks. (16) Belt tensioning device. (17) Shaft locking assembly. (18) $\frac{1}{15}$ HP gearmotor. (19) Test object. (20) 1 in. thick lucite window.

traction characteristics which prevent any possibility of slippage, as might be found in a typical flat-belt crowned-pulley drive.

Owing to the fact that the belts span a distance of almost 80 in. it was necessary to provide support to prevent their sagging and bowing in the test section. This was accomplished by guiding the belt across a flat stainless steel sheet having overhanging grips on the top and bottom.

As shown in figure 1, the entire belt and pulley assembly is supported in such a manner that it is free to move in a transverse direction thereby providing for a continuously variable gap width. Once the width is established, the assembly may be locked in place.

Performance characteristics of the shear-flow apparatus

Following the design and construction of the shear-flow apparatus, an experimental programme was initiated to quantitatively define the behaviour of the flow fields which could be generated. Of prime interest in this study was the case in which the belts were set to move in opposite directions at equal speeds, since, ideally, this should give rise to a linear shear flow within the test section.

As shown in figure 1 the tank was partially filled with water, on which was floated a highly water insoluble viscous Newtonian polymer, Polybutene no. 8. The purpose for this was to minimize the presence of vertical velocity gradients in the polymer, thereby enhancing the two-dimensionality of the flow in the test section.

Each gearmotor was connected to solid state variable speed controllers which provided extremely close speed regulation of the belts. Furthermore, the belt velocity was constantly monitored by observing to what extent the degree of synchronization could be maintained between an electronic strobotac and a grooved disk which, as shown in figure 1, was fastened to each gearmotor shaft.

Prior to measuring velocity profiles quantitatively, a number of rather general qualitative observations were made in order to establish the gross character of the flows generated by the apparatus. To accomplish this, a mount was constructed on which a camera was placed in such a way that the motion in the polymer could be photographed from above, as shown in figure 1. The camera lens was kept parallel to the fluid surface and could be adjusted to any desired height. This made it possible to obtain photographs at all levels in the tank, from the air interface all the way down to the water interface. By sweeping a small piece of fine mesh stainless steel screen through the test section, a large number of very tiny bubbles were produced, which in the viscous polymer ($\sim$ 2–3 poise) had such an extremely small rate of rise, that they could be used conveniently as tracers for obtaining streaklines and velocity profiles. This was accomplished by taking time exposure photographs of these bubbles with the aid of illumination, at right-angles to the camera lens, produced by synchronized electronic strobotacs placed at each end window.

A typical photograph of the streamline patterns generated by the shear-flow apparatus is shown in figure 2 (plate 1). Here a dark circle corresponding to a $\frac{1}{2}$ in. diameter has been superimposed on the picture in order to give an idea of how the scale of the flow field compares to the size of the cylinder used in the

experiments. Also, it represents the geometric centre of the tank when viewed from above. The gap width is about 22 in., hence, the photograph spans approximately half the test section. Clearly, although the flow is parallel to the belts away from the centre of the tank, it appears to possess a transverse velocity component close to the ideal location of the stagnation streamline. Fortunately, it will be seen that the presence of these secondary motions which, as shown by Robertson (1969), are due to end effects, is of little consequence, since the corresponding velocities are extremely weak.

Velocity profiles

Using the bubble-strobotac technique, velocity profiles were obtained at two different heights in the polymer. The results, shown in figures 3 and 4, provide good evidence that the velocity profile is very linear at the centre of the test

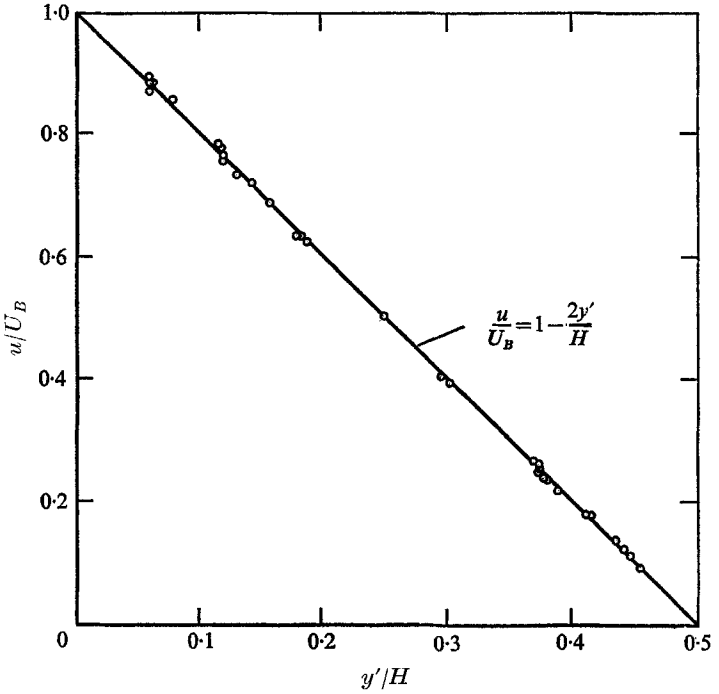

FIGURE 3. Velocity profile: 1·5 in. below polymer surface, $2U_BH/\nu = 158$.

section, and is in fact independent of vertical location. These measurements are for an aspect ratio A of 2, where

$$A = L/H,$$

L being the test section half-length, and H the gap width.

These results certainly demonstrate the pronounced effectiveness of the aqueous layer in helping to generate a truly two-dimensional flow. Furthermore, they strongly indicate that the presence of crossflow has a negligible effect on the longitudinal velocity component and that any noticeable curvature of the streamline paths over the region of the test field could not be detected when measuring velocities. Therefore, with reference to future experiments, one would expect

that an object placed at the geometric centre of the apparatus would find itself in an environment which, for all intents and purposes, would be identical locally to the idealized dimensional linear shear flow

$$u = U_B(1 - 2y'/H),$$

where y' is the dimensional transverse distance measured from one of the belts and U_B is the speed of the belts.

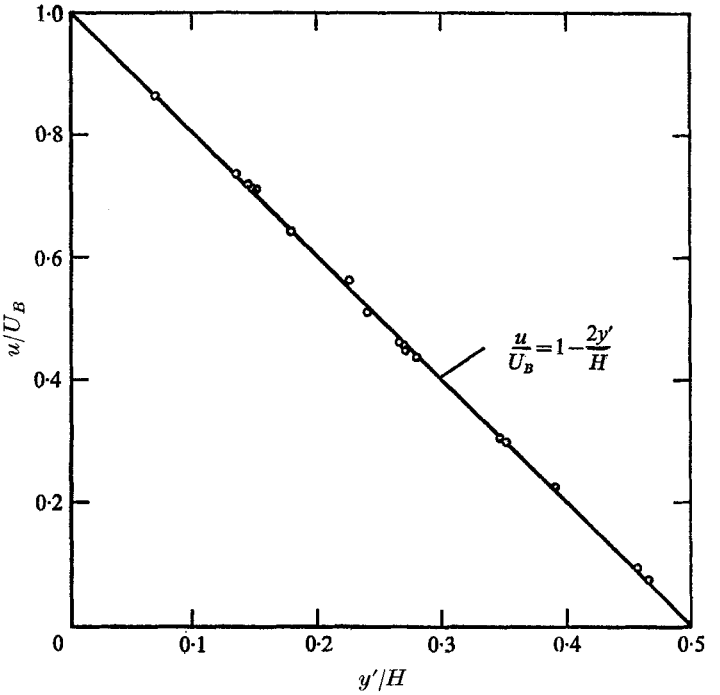

FIGURE 4. Velocity profile: 6·5 in. below polymer surface, $2U_BH/\nu = 158$.

Shear flow past a circular cylinder

The cylinder used in these experiments was fabricated from a $\frac{1}{2}$ in. diameter aluminium rod and was placed in the apparatus as shown in figure 1. At the bottom-viewing window, it passed through a rotating seal and then engaged a timing-belt drive system, while at the top, it passed through the centre of an 8×8 in. piece of lucite, which in turn was fastened to two aluminium support bars spanning the width of the tank. No bearing or other device to permit ease of rotation was fitted into the lucite; the rod simply revolved against the lucite surface to which a thin coat of machine oil had been applied. In this way, photographs could be taken from above without having any obstructions present to obscure the flow patterns.

The experiments covered the range of cylinder Reynolds numbers

$$6 \times 10^{-4} \leqslant R \leqslant 0{\cdot}7,$$

where, as in (6),

$$R = \frac{Sa^2}{\nu} = \frac{2U_Ba^2}{H\nu}.$$

Also, in all cases to be described, H was set equal to 19·8 in.

(i) $\Omega = 0$. Shown in figure 5 (plate 2) is a typical photograph of the experimental streamline patterns for a stationary cylinder, obtained by means of the techniques described above. In turn, these photographs were magnified and then used to effect a comparison between experimentally observed and theoretically predicted streamlines. Thus, a particular tracer bubble was first selected, its coordinates with respect to the centre of the cylinder were determined along its

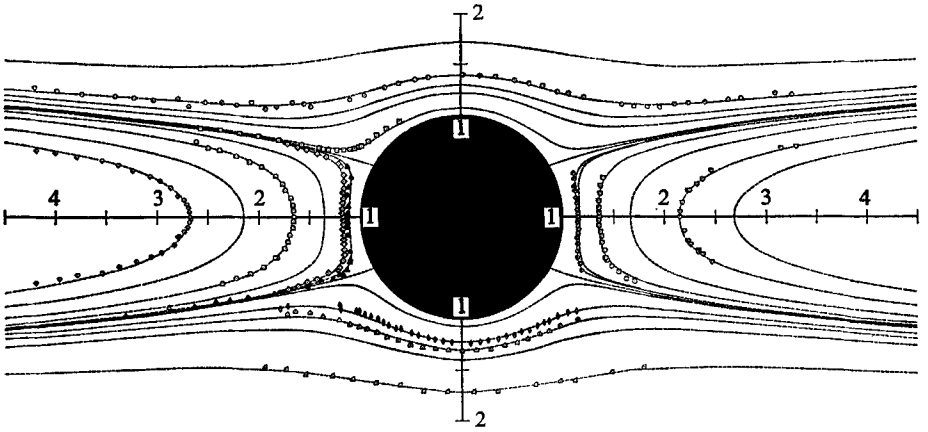

FIGURE 6. Comparison between theory and experiment for the shear flow past a stationary circular cylinder, $\Omega = 0$.

ψ	
$\theta = 0°, 180°$	$\theta = 90°, 270°$
0 (surface)	0 (surface)
−0·005	0·01
−0·01	0·06
−0·04	0·11
−0·10	0·18
−0·19	0·53
−0·28	

TABLE 1. Values of the stream function for the theoretical streamlines shown in figure 6

path and a value for the stream function corresponding to that particular streamline was assigned by averaging the individual values of ψ computed according to (4). The data were then superimposed on the theoretical streamline as given by (4) using this same value for the streamfunction ψ. The results are shown in figure 6. Here, the dashed lines represent the theoretical streamlines, for which the corresponding values of the stream function are given in table 1 in ascending order along the x and y axes.

Undoubtedly the most prominent feature of this flow is the appearance of two recirculating wakes on either side of the cylinder. As shown in figure 6, the theoretical $\psi = 0$ streamline intersects the cylinder surface at $\theta = \pm 30°$, a prediction which is obviously borne out by figure 5. Clearly, the theoretical and experimental streamlines are in excellent agreement throughout the flow field covered by the photographs.

(ii) $\Omega = \frac{1}{4}$. When the rotational speed of the cylinder falls into the range $0 < \Omega < \frac{1}{2}$, a fundamental change in the structure of the flow field occurs due to the appearance of a region of closed streamlines which surround the object. This is evident from the theoretical streamline patterns depicted in figure 7 for

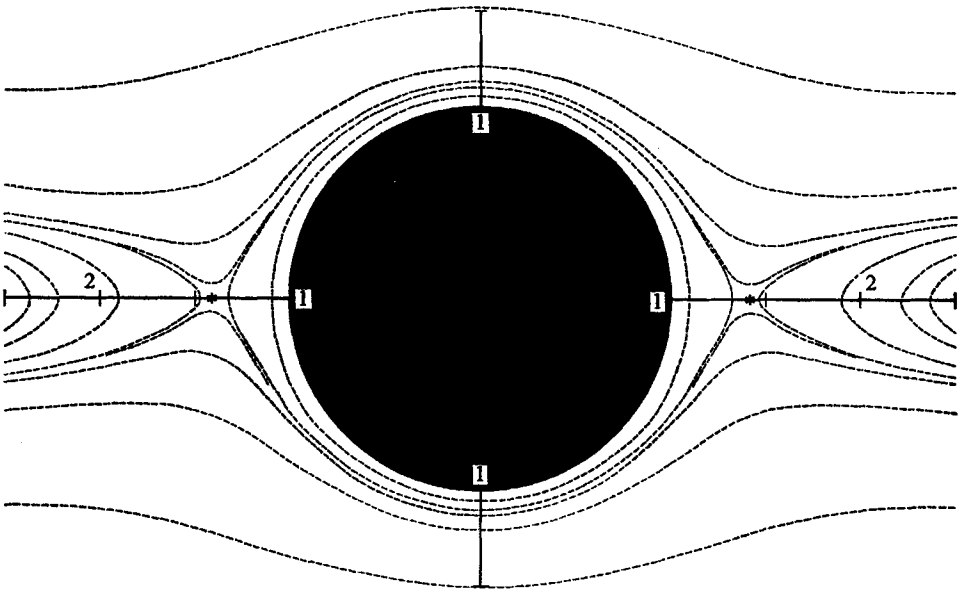

FIGURE 7. Theoretical streamlines for the shear flow past a rotating circular cylinder, $\Omega = \frac{1}{4}$.

ψ	
$\theta = 0°, 180°$	$\theta = 90°, 270°$
0 (surface)	0 (surface)
0·020	0·020
0·038	0·038
0·03836...(stagnation point)	0·050
0·020	0·010
0	0·40
−0·10	

TABLE 2. Values of the stream function for the theoretical streamlines shown in figure 7; note that the streamline which is only partially visible near the stagnation point corresponds to $\psi = 0{\cdot}039$

$\Omega = \frac{1}{4}$. Values of the stream function corresponding to these theoretical streamlines, which cross the x and y axes in an ascending order, are listed above in table 2.

It should be noted that, by virtue of the rotation of the cylinder, the wake regions have been displaced from the surface of the object; however, on account of (7), their width is still proportional to $(\ln r)^{\frac{1}{2}}$ for r sufficiently large. Unfortunately, owing to the presence of the stagnation points in this flow, it was not

possible to obtain quantitative data using the present experimental techniques since the bubble tracers tended to rise in regions where the fluid velocities were small. However, as shown in figure 8 (plate 3), the observed flow structure is in

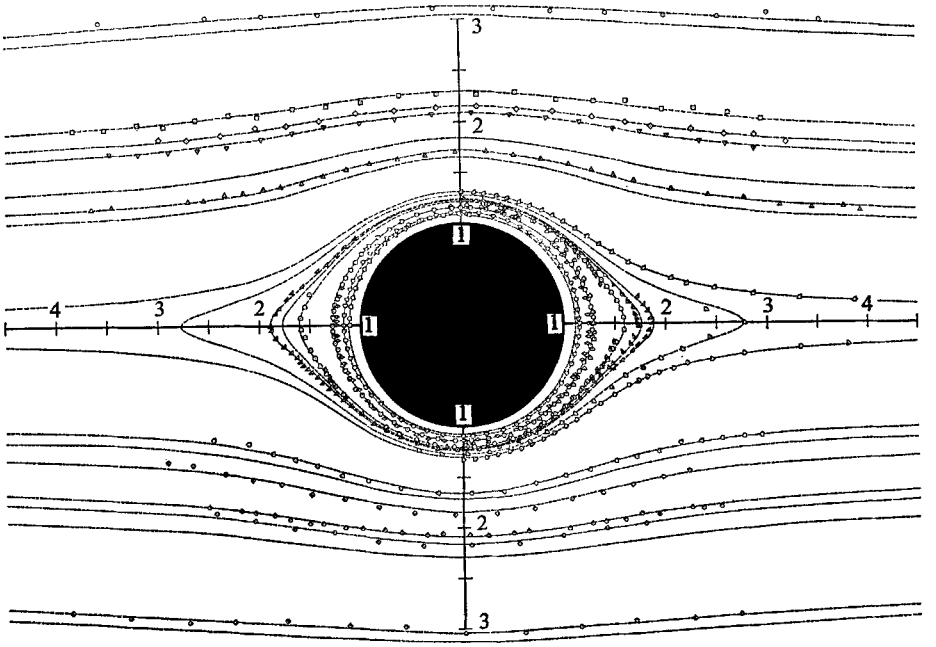

FIGURE 10. Comparison between theory and experiment for the shear flow past a freely rotating circular cylinder, $\Omega = \frac{1}{2}$.

ψ	
0 (surface)	0·70
0·050	0·81
0·065	1·01
0·10	1·48
0·15	1·63
0·17	1·93
0·18	3·86
0·22	4·16
0·25	

TABLE 3. Value of the stream function for the stream lines shown in figure 10

good qualitative agreement with the theoretical predictions in that it can be seen to possess the same important features depicted in figure 7, namely, the wakes, the region of closed streamlines, and, barely visible, the two stagnation points.

(iii) $\Omega = \frac{1}{2}$. Shown in figure 9 (plate 4) is a typical experimental streamline pattern which resulted when Ω was set equal to $\frac{1}{2}$, the value corresponding to free rotation. As in (i), such pictures were used to compute point values of the

stream function along a given bubble path which, in most cases, were found to be within a few per cent of the experimentally obtained mean value for a given streamline. The results of such measurements, which are more extensive than those reported by Cox *et al.* (1968) in that they include more streamlines and a substantially larger area surrounding the cylinder, are shown in figure 10 where the dashed lines represent once again the streamlines given by the Stokes solution to this problem (4). The value of the stream function for each streamline in ascending order is given in table 3.

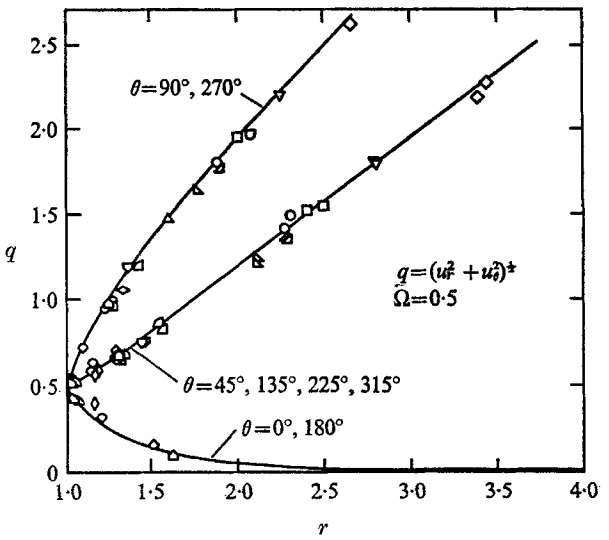

FIGURE 11. Measured values of the speed q for $\Omega = \frac{1}{2}$.

Clearly the agreement between theory and experiment is excellent. However, a somewhat more sensitive test involves the comparison between theoretically and experimentally determined speeds along a given streamline. To this end, local values of the speed were measured at angular increments of 45° from the same photographs used in obtaining the data presented in figure 10. The results are shown in figure 11, where the solid lines represent the theoretical values of the speed q, as computed from (4).

Similar symbols on the figure refer to data that were obtained from the same streamline.

The excellent agreement between theory and experiment indicate, of course, that the tracer bubbles were moving with the theoretical speed along their entire path, for streamlines both outside and inside the circulating region. This agreement is all the more satisfying considering that the measured value of the speed was actually an average quantity taken over several degrees of arc.

(iv) $\Omega = \frac{3}{2}$. When the speed of the cylinder was allowed to exceed that required for free rotation, $\Omega > \frac{1}{2}$, the resulting experimental flow pattern was as shown in figure 12 (plate 5). Again, as seen in figure 13, there is complete agreement between the theory, represented as dashed lines, and the experimental data.

Values of the stream function corresponding to the streamlines in figure 13 are given in table 4 in ascending order along the y axis.

As in the $\Omega = \frac{1}{2}$ case, speeds were also measured along streamlines at 45° increments. These results are presented in figure 14, where again the solid lines refer to the speeds as given by the creeping flow solution (4). Once more, like symbols identify data that were obtained from the same streamline. Clearly, as before, the comparison between experiment and theory is excellent.

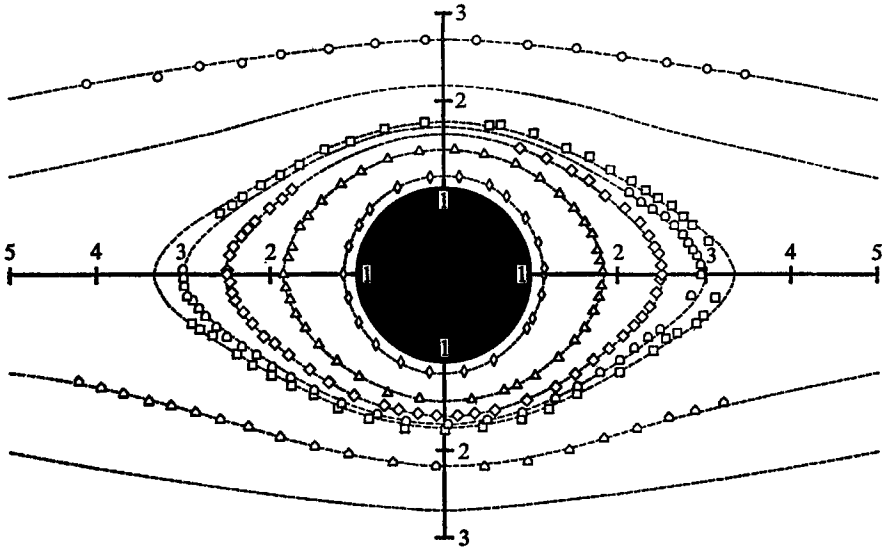

FIGURE 13. Comparison between theory and experiment for the shear flow past a rotating circular cylinder, $\Omega = \frac{3}{2}$.

ψ	
$\theta = 90°$	
0 (surface)	1·32
0·21	1·43
0·79	2·44
1·14	3·92

TABLE 4. Values of the stream function for the streamlines shown in figure 13

In conclusion, the experimental evidence which has been presented shows that the Stokes solution accurately describes the two-dimensional low Reynolds number flow past a circular cylinder for arbitrary rotational speeds when the motion at infinity is a uniform simple shear. However, this experimental verification applies only to the inner region, since the presence of end effects in the shear-flow apparatus made it impossible to obtain even a qualitative investigation of the structure of regions far from the cylinder. Fortunately, though, as shown in § 5, many important aspects of the nature of the flow in the Oseen region have been clarified by analytically investigating the problem through the use of the technique of matched asymptotic expansions.

This work was supported in part by grants from the National Science Foundation and the Petroleum Research Fund administered by the American Chemical Society. The authors are indebted to Mr Charles Hoard for his assistance during the initial phases of the experimental programme, and to Mr Sal Bravo who helped to direct the fabrication of the bulk of the shear-flow apparatus and gearmotor mounts. Also, we would like to thank Mr Gunther Kuhn for his invaluable suggestions regarding the design and construction of the apparatus.

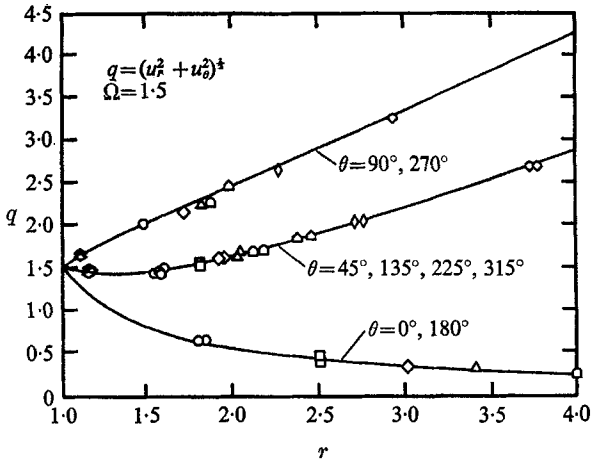

FIGURE 14. Measured values of the speed q for $\Omega = \frac{3}{2}$.

REFERENCES

BRETHERTON, F. P. 1962 Slow viscous motion round a cylinder in a simple shear. *J. Fluid Mech.* **12**, 591.

COX, R. G., ZIA, I. Y. Z. & MASON, S. G. 1968 Particle motions in sheared suspensions. XXV. Streamlines around cylinders and spheres. *J. Colloid Interface Sci.* **27**, 7.

DARABANER, C. L., RAASCH, J. K. & MASON, S. G. 1967 Particle motions in sheared suspensions. XX. Circular cylinders. *Can. J. Chem. Engng* **45**, 3.

DEARDORFF, J. W. 1963 On the stability of viscous plane Couette flow. *J. Fluid Mech.* **15**, 623.

FRANKEL, N. A. & ACRIVOS, A. 1968 Heat and mass transfer from small spheres and cylinders freely suspended in shear flow. *Phys. Fluids*, **11**, 1913.

GIESEKUS, H. 1962 Strömungen mit konstanten Geschwindigkeitsgradienten und die Bewegung von darin suspendierten Teilchen. *Rheologica Acta*, **2**, 112.

KOHLMAN, D. L. & MOLLO-CHRISTENSEN, E. 1965 Measurement of drag of cylinders and spheres in a Couette-flow channel. *Phys. Fluids*, **8**, 1013.

KOHLMAN, D. L. 1963 Experiments on cylinder drag, sphere drag, and stability in rectilinear Couette flow. *Fluid Dynamics Report*, **63–1**, Massachusetts Institute of Technology.

MASON, S. G. & TREVELYAN, B. J. 1951 Particle motions in sheared suspensions. Part I. Rotations. *J. Colloid Sci.* **6**, 354.

MORSE, P. M. & FESHBACH, H. 1953 *Methods of Theoretical Physics, Part II.* New York: McGraw-Hill.

PROUDMAN, I. & PEARSON, J. R. A. 1957 Expansions at small Reynolds numbers for the flow past a sphere and a circular cylinder. *J. Fluid Mech.* **2**, 237.

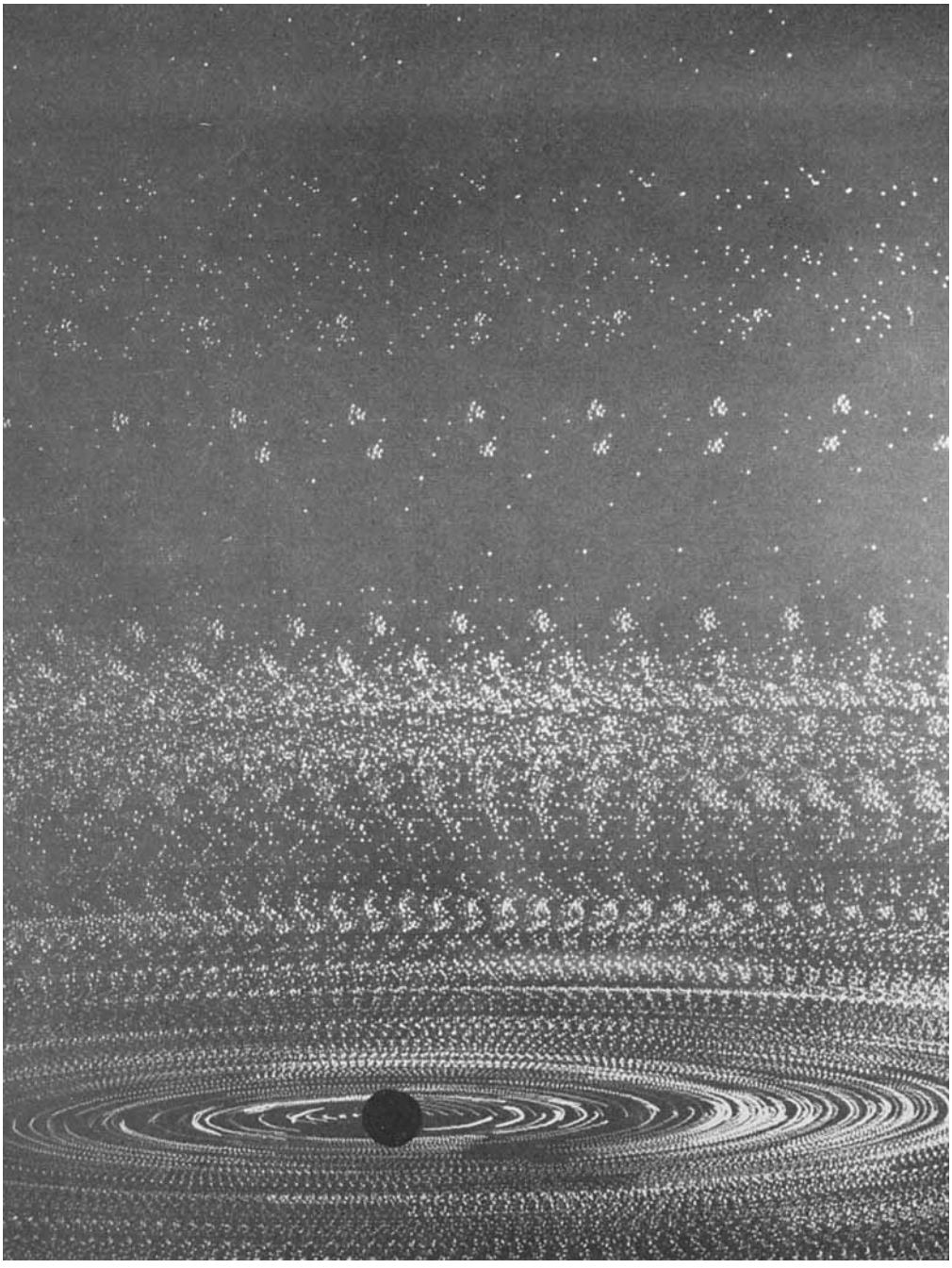

FIGURE 2. Test section streamline patterns in the absence of a test object. (Belt velocity: $U_B = 3{\cdot}0$ in./sec.)

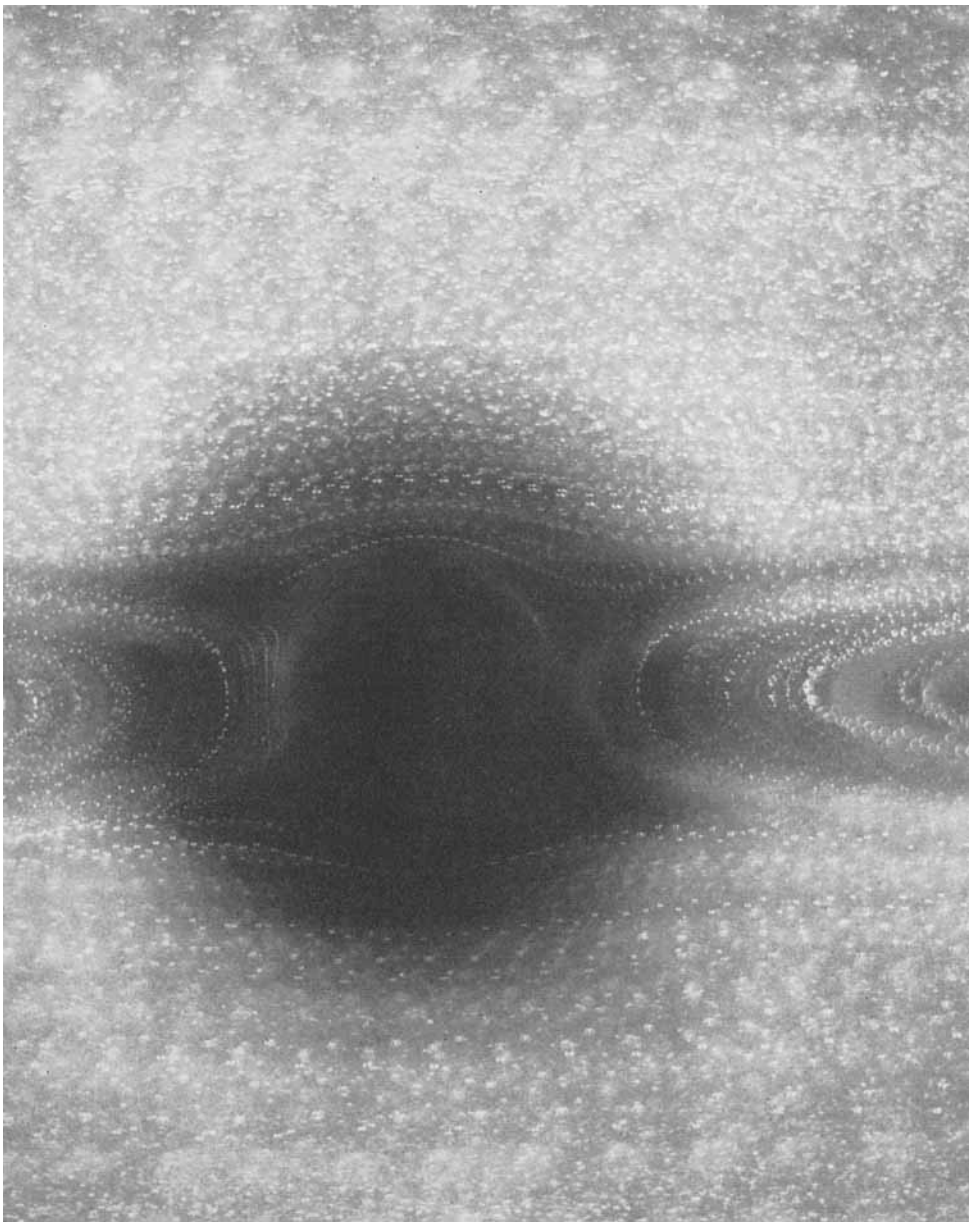

FIGURE 5. Shear flow past a stationary circular cylinder, $\Omega = 0$, $R = 0{\cdot}047$.

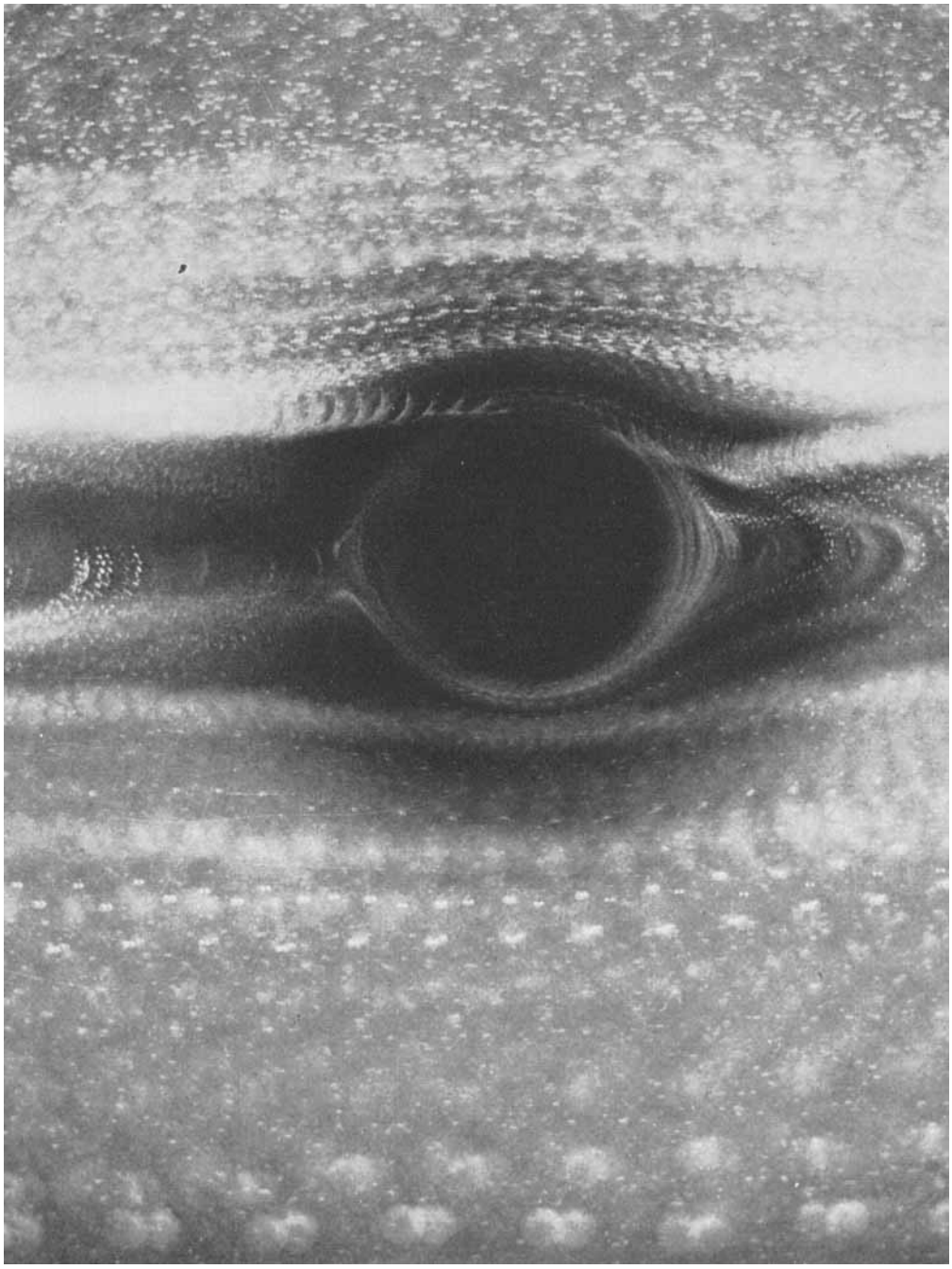

FIGURE 8. Shear flow past a rotating circular cylinder, $\Omega = \frac{1}{4}$, $R = 0{\cdot}047$.

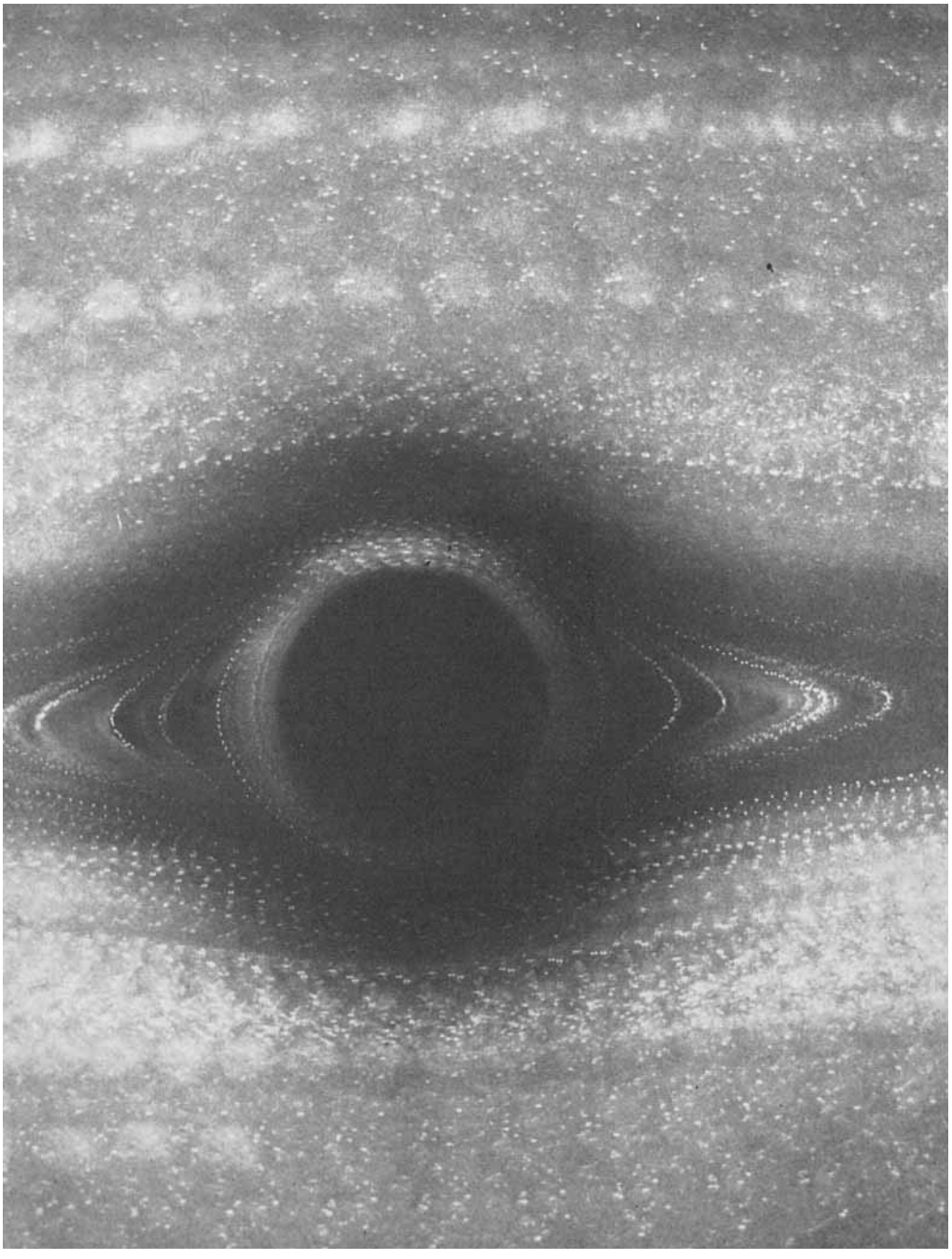

FIGURE 9. Shear flow past a freely rotating circular cylinder, $\Omega = \frac{1}{2}$, $R = 0{\cdot}047$.

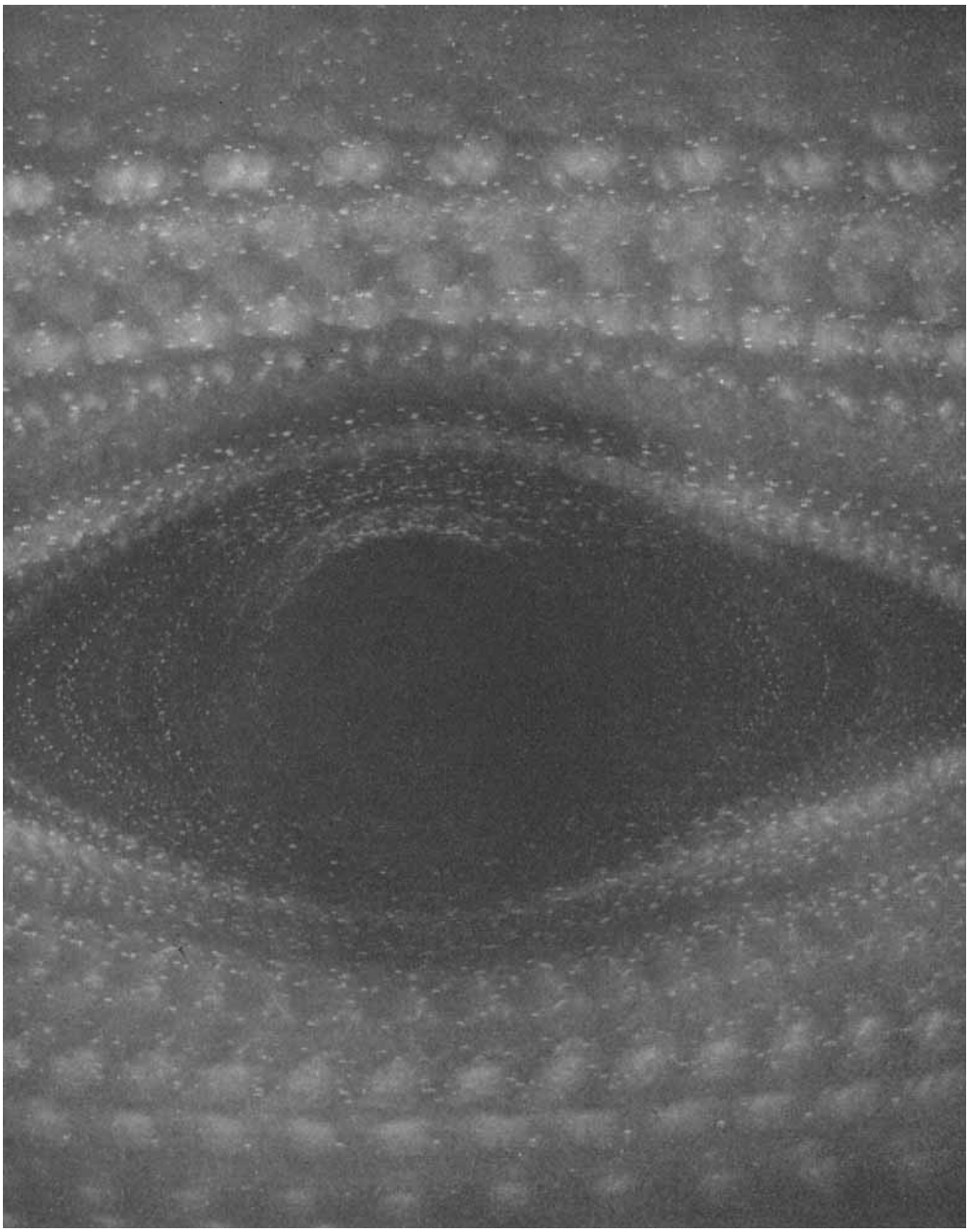

FIGURE 12. Shear flow past a rotating circular cylinder, $\Omega = \frac{3}{2}$, $R = 0{\cdot}047$.